A Spectrum-Efficient Multicarrier CDMA Array-Receiver with Diversity-Based Enhanced Time and Frequency Synchronization

Besma Smida, *Member, IEEE,* Sofiène Affes, *Senior Member, IEEE,* Jun Li, and Paul Mermelstein, *Fellow, IEEE*

***Abstract*— This paper proposes a spectrum-efficient spatio-temporal array-receiver for multi-carrier CDMA systems named MC-STAR. First, we derive a new post-correlation model for MC-CDMA that characterizes the structure of the channel in space, time and frequency. Based on this model, we introduce a new multi-carrier array-receiver with rapid and accurate joint synchronization in time and frequency. There, we exploit jointly the spatial, temporal and frequency diversities as well as the intrinsic inter-carrier correlation (termed hereafter *frequency gain*) to improve the channel identification and the synchronization operations. In addition, based on a new link/system-level performance analysis, with a band-limited chip waveform assumption, we provide a comparative performance study of MC-STAR over two multi-carrier CDMA air-interface configurations, namely MT-CDMA and MC-DS-CDMA, in the most realistic operating conditions. Link/system-level results confirm the advantages of MT-CDMA in increasing throughput and bandwidth efficiency. The current trend is to design radio air-interfaces with flat fading subcarriers. In contrast, with MC-STAR we show that the positive effects of multipath diversity and *frequency gain* over large strongly-overlapping subcarriers is more significant than the negative effects of multipath and multi-carrier interference.**

***Index Terms*— Channel identification, synchronization, carrier frequency offset recovery, antenna arrays, code division multiple access (CDMA), multicarrier systems, MT-CDMA, MC-DS-CDMA.**

I. Introduction

ONE important challenge for future wireless networks is the design of appropriate transceivers that can reliably transmit high data rates at a high bandwidth efficiency. Multi-carrier (MC)-CDMA systems in particular have received considerable attention, because they have the attractive feature of high spectral efficiency and because they can be easily implemented using the fast fourier transform (FFT) without significantly increasing the transmitter and receiver complexities [1].

Manuscript received October 26, 2005; revised July 31, 2006 and November 7, 2006; accepted January 8, 2007. The associate editor coordinating the review of this paper and approving it for publication was D. Gesbert. This work was supported by a Canada Research Chair in High-Speed Wireless Communications and the NSERC Strategic Partnership Grants Program. This paper was presented in part at the IEEE SPAWC 2003 and IEEE ICC 2005 conferences.

B. Smida is with the School of Engineering and Applied Sciences, Harvard University, Cambridge, MA (e-mail: bsmida@seas.harvard.edu).

S. Affes and P. Mermelstein are with INRS-EMT, University of Quebec, Montreal, Quebec, Canada (e-mail: {affes, mermel}@emt.inrs.ca).

J. Li is with the Centre de Recherches Mathmatiques, Université de Montréal, Montreal, Quebec, Canada (e-mail: li@crm.umontreal.ca).

Digital Object Identifier 10.1109/TWC.2007.05842.

The multi-carrier systems include different combinations of multi-carrier modulation [accomplished by orthogonal frequency division multiplex (OFDM)] and direct-sequence code division multiple access (DS-CDMA). This combination provides both high data-rate transmission and multiple access capabilities. An excellent overview of the different multi-carrier CDMA systems is found in [1]. They can be divided into two categories of multi-carrier CDMA: one combines multi-carrier modulation with frequency-domain spreading, the other transmits several DS-CDMA waveforms in parallel with the spreading operation performed in time. The transmitter proposed here belongs to the second group (i.e., time spreading, study of the first group is beyond the scope of this paper). In the second group, transceivers can be divided into MC-DS-CDMA and multitone (MT)-CDMA, the difference between the two being the subcarrier frequency separation. They can be unified in a family of generalized MC-DS-CDMA transceivers, defined in [2], using a range of frequency spacings, parameterized by λ, between two adjacent subcarriers. In this work we adopt this general view and simply refer to it as MC-CDMA in the remainder of the paper unless otherwise required.

However promising, challenges remain before MC-CDMA can achieve its full potential. MC-CDMA is sensitive to the signal distortion generated by the imperfect frequency down-conversion at the receiver due to local oscillator frequency offset. It has been found that carrier frequency offset (CFO) gives rise to a reduction of the useful signal power and to the inter-carrier interference (ICI) [3]. In addition to the degradation induced by the CFO, an MC-CDMA signal experiences inter-symbol interference (ISI) and ICI caused by the multipath effect [4]. In order to enjoy all the benefits of multi-carrier transmission, two key tasks must be successfully accomplished: 1) multipath channel identification and equalization and 2) carrier frequency offset estimation and recovery (CFOR). Carrier synchronization and channel identification have traditionally been treated as separate problems. Most research on channel identification implicitly assumes that the carrier offset has been properly compensated [5]. Similarly, many existing CFOR techniques consider only flat channels [6], [7], [8]. Some works have investigated the joint estimation of multipath and carrier offset for multi-carrier CDMA systems with frequency spreading [9], [10], but no such investigations are available for MC-DS-CDMA or MT-CDMA systems (i.e., time spreading only).

We propose a new MC-CDMA receiver that supports both MC-DS-CDMA and multitone (MT)-CDMA. It performs blind channel identification and equalization as well as fast and accurate joint synchronization in time and frequency using a simple linear regression (LR) technique. With reference to our starting configuration, the original STAR receiver [11] that showed a significant performance advantage over Rake-type receivers both in channel identification and synchronization for DS-CDMA [12], we summarize our main contributions as follows:

- Based on non-trivial mathematical derivations, we extend the post-correlation model (PCM) originally developed for single-carrier DS-CDMA STAR [11] to MC-CDMA air-interfaces by characterizing the structure of the channel in space, time, and frequency. This model is named multi-carrier PCM (MC-PCM) and it applies to MT-CDMA, MC-DS-CDMA, and DS-CDMA.
- We resort to an essential and new transform of the channel estimate over each subcarrier that allows, in a preliminary step, direct and easy application of single-carrier STAR independently over each subcarrier.
- To overcome the sensitivity of MC-CDMA to the CFO, we introduce over each carrier a new joint time and frequency synchronization module based on a simple LR technique that is fast and accurate.
- Independent application of single-carrier STAR over each subcarrier is far from optimal in a multi-carrier transmission. We hence exploit the inter-carrier correlation, intrinsic to a multi-carrier system, to implement joint multi-carrier channel identification and synchronization operations with significantly improved performance. Based on MC-PCM, parameters common to subcarriers can be estimated more accurately by averaging their estimates over all subcarriers. Other channel parameters, such as the fading coefficients, are correlated but not identical over all subcarriers. Therefore, combining them may not achieve the expected performance enhancement. We hence introduce a moving average technique over strongly-correlated subcarriers. All the parameter estimates are equally weighted and combined through summation. Since estimation errors can be assumed uncorrelated across subcarriers, joint estimation by averaging provides a type of *frequency (or subcarrier) gain*[1] in a joint multi-carrier estimation process. The new multi-carrier receiver is named MC-STAR. To the best of our knowledge, it is also the first receiver that exploits simultaneously spatial, temporal and frequency diversities in channel parameter estimation and CFO recovery. Simulation results confirm the accuracy of the joint time/frequency synchronization.
- We derive a performance analysis of MC-STAR over the two multi-carrier CDMA air-interface configurations, MT-CDMA and MC-DS-CDMA, with a band-limited square-root raised cosine pulse. Note that the chip waveform is an important system parameter for DS-CDMA and MC-DS-CDMA [13][14]. Therefore, the effect of both time-limited and band-limited chip waveforms on the performance of DS-CDMA and MC-DS-CDMA have been investigated. However, for all the MT-CDMA systems found in the literature, a time-limited waveform is generally employed [2][16][17][18]. Band-limitation filtering causes the chip waveforms to disperse over the time axis and overlap one another, which increases the difficulty of calculation of the variance of the interference. Since we consider a practical square-root raised cosine pulse, we have derived the performance of MC-CDMA (including MC-DS-CDMA and MT-CDMA) with a band-limited square-root raised-cosine waveform.
- We provide a comparative performance study of MC-STAR over the two multi-carrier CDMA air-interface configurations MT-CDMA and MC-DS-CDMA using a very realistic link-level simulation setup and an analytical system-level evaluation. Link-level simulation setups take into account time and frequency mismatch, imperfect power control, channel identification errors, etc by implementing joint synchronization, channel identification, power control and combining, etc. This is the first evaluation work by simulations that takes such a realistic step of reproducing most of the real-world operating conditions.

Link/system-level results confirm the advantages of MT-CDMA in increasing throughput and bandwidth efficiency. The current trend is to design radio air-interfaces with flat fading subcarriers. In contrast, with MC-STAR we show that the positive effects of multipath diversity and *frequency gain* over large strongly-overlapping subcarriers is more significant than the negative effects of multipath and multi-carrier interference.

II. System Model and Assumptions

A. MC-CDMA Transmitter

The input information sequence is first converted into $N_c = 2K + 1$ parallel data sequences $b_{-K,n}, \ldots, b_{0,n}, \ldots, b_{K,n}$ where n is the time index (see Fig. 1). The data $b_{k,n} \in C_{\mathcal{M}}$ (i.e., constellation set) is $\mathcal{M}$-PSK modulated and differentially[2] encoded at rate $1/T_{MC}$, where $T_{MC} = N_c \times T$ is the symbol duration after serial/parallel (S/P) conversion and T is the symbol duration before S/P. The resulting S/P converter output is then spread with a long spreading code $c(t)$ at a rate $1/T_c$. The spreading factor, defined as the ratio between the chip rate and the symbol rate is $L = \frac{T_{MC}}{T_c}$. We consider square-root raised-cosine chip pulses with rolloff factor β. Closed-loop power control is taken into account at the transmitter by the amplification factor $a_k(t)$. All the data are then modulated in baseband by the inverse discrete Fourier transform (IDFT) and added to obtain the multi-carrier signal. A guard interval $T_g = L_g \times T_c$ is then inserted between symbols to avoid intersymbol interference caused by multipath fading[3]. Finally the signal is transmitted after pulse shaping and radio-frequency up-conversion. The modulated subcarriers are orthogonal over the symbol duration T_{MC}. The frequency corresponding to the k-th subcarrier is $f_k = \lambda \times k/T_{MC}$. The transmitter belongs to the family of MT-CDMA if λ is set to 1, and to the class of MC-DS-CDMA if λ is set to L (see

[1]By analogy to the well known antenna gain one can achieve by averaging and hence reducing uncorrelated noise over sensors.

[2]The pilot symbols could be used for coherent modulation and detection [19], but that is beyond the scope of this paper.

[3]Simulations will later indicate that the guard interval can be eliminated when using MC-STAR, thereby leading to higher spectral efficiency.

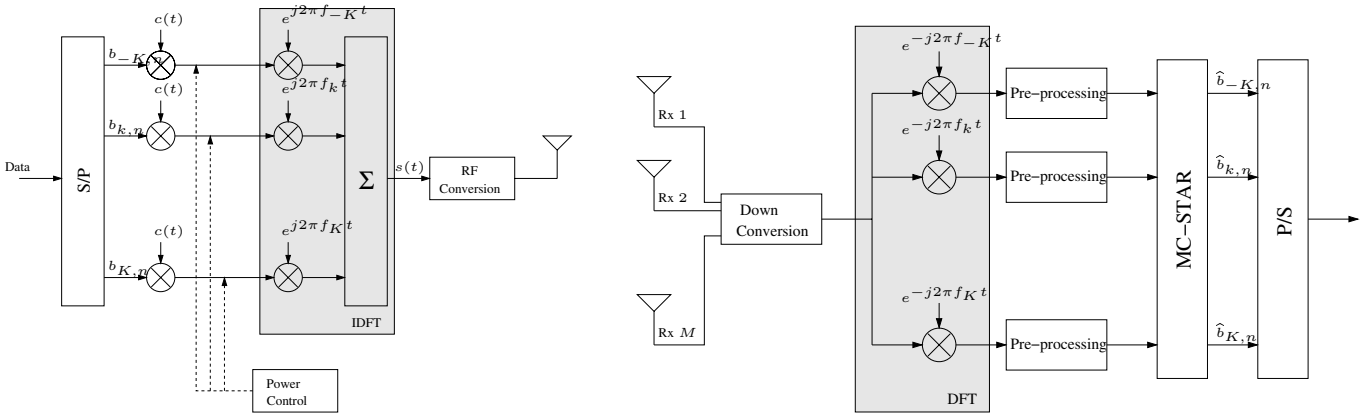

Fig. 1. Block diagram of the MC-CDMA transmitter and receiver (pulse shape filtering is implemented at both transceiver ends).

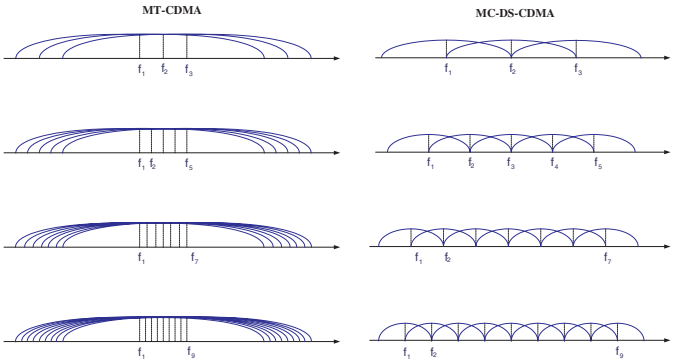

Fig. 2. Different configurations of MT-CDMA and MC-DS-CDMA within the same bandwidth.

resulting signal spectra in Fig. 2). The transmitted bandwidth is:

$$BW = \frac{(N_c - 1)\lambda}{T_{MC}} + \frac{(1+\beta)}{T_c}. \quad (1)$$

B. Channel Model

We consider transmission to M receiving antennas. The channel is assumed to be a slowly varying frequency selective Rayleigh channel with delay spread $\Delta\tau$. We note here that the large-scale path-loss that includes free-space path-loss and shadowing is the same for all subcarriers. Moreover, the number of resolvable paths P and their propagation time-delays $\tau_1(t), \ldots, \tau_P(t)$ depend on the reflecting objects and scatterers and, therefore, can be assumed equal for all subcarriers [20]. We assume correlated Rayleigh channels across subcarriers and adopt the approach proposed in [21] to generate them. We also assume that the received channel multipath components across the M antennas are independent. The M-dimensional complex low-pass equivalent vector representation of the impulse response experienced by subcarrier k is hence:

$$H_k(t) = \frac{\rho(t)}{r^d(t)} \sum_{p=1}^{P} \mathcal{G}_{k,p}(t)\delta(t - \tau_p(t)), \quad (2)$$

where $\rho(t)$ and $r^d(t)$ model the effects of shadowing and path loss, respectively, $r(t)$ is the distance from the user to the base-station and d is the path loss exponent. For an MC-CDMA system, the received signal is the superposition of signals from all subcarriers. Hence the M-dimensional observation vector received by the antenna array can be expressed as follows:

$$\begin{aligned} X(t) &= \sum_{k=-K}^{K} H_k(t) \otimes a_k(t) b_k(t) c(t) e^{j2\pi f_k t} + N(t) \\ &= \frac{\rho(t)}{r^d(t)} \sum_{p=1}^{P} \sum_{k=-K}^{K} \mathcal{G}_{k,p}(t) a_k(t-\tau_p) b_k(t-\tau_p) \\ &\quad \cdot c(t-\tau_p) e^{j2\pi f_k (t-\tau_p)} + N(t) \\ &= \sum_{k=-K}^{K} \psi_k(t) \sum_{p=1}^{P} G_{k,p}(t) \epsilon_{k,p}(t) b_k(t-\tau_p) \\ &\quad \cdot c(t-\tau_p) e^{j2\pi f_k (t-\tau_p)} + N(t), \end{aligned} \quad (3)$$

where $\otimes$ denotes time convolution. The noise term $N(t)$ includes the thermal noise received at the antenna as well as the in-cell and out-cell interference. Along the p-th path, $G_{k,p}(t) = \mathcal{G}_{k,p}(t)(\sqrt{M}/||\mathcal{G}_{k,p}(t)||)$ is the propagation vector over the k-th subcarrier with norm $\sqrt{M}$ and $\epsilon^2_{k,p}(t) = ||\mathcal{G}_{k,p}(t)||^2 / \sum_{p=1}^{P} ||\mathcal{G}_{k,p}(t)||^2$ is the fraction of the total received power on the k-th subcarrier $\psi_k(t)^2 = \left(\rho(t)/r^d(t)\right)^2 a_k^2(t) \sum_{p=1}^{P} ||\mathcal{G}_{k,p}(t)||^2/M$.

C. Extension of the Post-Correlation Model to MC-CDMA Air-Interfaces

We provide in this section an extension of the post correlation model derived for DS-CDMA systems in [11], to the multi-carrier case. To retrieve $b_{k,n}$ for the k-th subcarrier at the receiver (see Fig. 1-(b)), we define the post-correlated observation vector of frame number n over a time-interval $[0, T_{MC})$ by

$$\begin{aligned} Z_{k,n}(t) &= \frac{1}{T_{MC}} \int_0^{T_{MC}} X(nT_G + t + t') e^{j2\pi\Delta f(nT_G+t+t')} \\ &\quad \cdot c(t' + nT_G) e^{-j2\pi f_k (t'+nT_G)} dt', \end{aligned} \quad (4)$$

where $T_G = T_{MC} + T_g$ and Δf models the CFO, which is assumed equal for all subcarriers. This is a realistic assumption since there is only one oscillator per receiver (see Fig. 1). As a result of the stationarity assumptions stated in section II-B, $Z_{k,n}(t)$ can be developed into Eq. (5). where $t'' = nT_G + t + t'$. We assumed in the development of Eq. (5) above that $\psi_{k'}(nT_G+t+t')$, $G_{k',p}(nT_G+t+t')$ and $\epsilon_{k',p}(nT_G+t+t')$ are constant during the interval $t' \in [0,\ T_{MC})$. We also considered that the frequency offset is small compared to the symbol rate ($\Delta f T_{MC} \ll 1$), thus $e^{j2\pi\Delta f(nT_G+t+t')} \simeq e^{j2\pi\Delta f n T_G}$ for $t' \in [0,\ T_{MC})$. After non-trivial mathematical derivations, a further

$$\begin{aligned} Z_{k,n}(t) &\approx \tfrac{1}{T_{MC}} e^{j2\pi\Delta f n T_G} \textstyle\sum_{k'=-K}^{K} \psi_{k'}(nT_G) \sum_{p=1}^{P} G_{k',p}(nT_G)\epsilon_{k',p}(nT_G) \int_0^{T_{MC}} b_{k'}(t''-\tau_p)c(t''-\tau_p) \\ &\quad .c(t'+nT_G)e^{j2\pi((f_{k'}-f_k)(nT_G+t')+f_{k'}(t-\tau_p))}dt' \\ &\quad + \tfrac{1}{T_{MC}} \textstyle\int_0^{T_{MC}} N(t'')c(t'+nT_G)e^{-j2\pi f_k(t'+nT_G)}dt'. \end{aligned} \tag{5}$$

$$\begin{aligned} Z_{k,n}(t) &\approx b_k(nT_G)\psi_k(nT_G)e^{j2\pi\Delta f n T_G} \textstyle\sum_{p=1}^{P} G_{k,p}(nT_G)\epsilon_{k,p}(nT_G)\rho_c(t-\tau_p)e^{j2\pi f_k(t-\tau_p)} + \text{ICI} + \text{ISI} \\ &\quad + \tfrac{1}{T_{MC}} \textstyle\int_0^{T_{MC}} N(nT_G+t+t')c(t'+nT_G)e^{-j2\pi f_k(t'+nT_G)}dt' \\ &\approx b_k(nT_G)\psi_k(nT_G)e^{j2\pi\Delta f n T_G} \textstyle\sum_{p=1}^{P} G_{k,p}(nT_G)\epsilon_{k,p}(nT_G)\rho_c(t-\tau_p)e^{j2\pi f_k(t-\tau_p)} + N_{k,n}(t). \end{aligned} \tag{6}$$

development of Eq. (5) gives Eq. (6) [24], where $\rho_c(t)$ is the correlation function of the chip pulse and $N_{k,n}(t)$ is the post-correlated noise of the frame number n, which includes the noise, the inter-carrier interference (ICI) and the inter-symbol interference (ISI) after despreading[4]. The noise is uncorrelated across subcarriers and hence the common parameters can be estimated more accurately by averaging their estimates over all subcarriers, yielding the so-called *frequency gain*.

We sample $Z_{k,n}(t)$ at a multiple of the chip rate over the interval $t \in [0,\ T_{MC})$[5]. The oversampling ratio k_s is defined as the number of samples per chip. In DS-CDMA and MT-CDMA systems we need no more than one sample per chip ($k_s = 1$). In contrast, in an MC-DS-CDMA system, a higher sampling frequency is necessary for the receiver. Hence, the smallest power-2 number greater than the number of subcarriers N_c is an adequate oversampling ratio for MC-DS-CDMA. Accordingly, we form the $M \times Lk_s$ block data matrix denoted by $\mathbf{Z}_{k,n} = [Z_{k,n}(0), Z_{k,n}(T_c/k_s), \ldots, Z_{k,n}((Lk_s-1)T_c/k_s)]$ as the post-correlated observation matrix:

$$\begin{aligned} \mathbf{Z}_{k,n} &= s_{k,n}\mathbf{H}_{k,n} + \mathbf{N}_{k,n} \\ &= s_{k,n}e^{j2\pi\Delta f n T_G}\mathbf{G}_{k,n}\boldsymbol{\Upsilon}_{k,n}\mathbf{D}_{k,n}^T + \mathbf{N}_{k,n} \\ &= s_{k,n}\mathbf{J}_{k,n}\mathbf{D}_{k,n}^T + \mathbf{N}_{k,n}, \end{aligned} \tag{7}$$

where $s_{k,n} = b_{k,n}\psi_{k,n}$ is the signal component on the k-th subcarrier and $\psi_{k,n}^2$ is the total power received over the k-th subcarrier. $\mathbf{H}_{k,n}$ is $M \times Lk_s$ spatio-temporal propagation channel matrix normalized to $\sqrt{M}$. $\mathbf{J}_{k,n} = e^{j2\pi\Delta f n T_G}\mathbf{G}_{k,n}\boldsymbol{\Upsilon}_{k,n}$ is the spatial response matrix. It corresponds to the propagation matrix $\mathbf{G}_{k,n}$ multiplied by the diagonal matrix of power partition over multipaths $\boldsymbol{\Upsilon}_{k,n} = \text{diag}\{\epsilon_{k,1,n}, \ldots \epsilon_{k,p,n}, \ldots \epsilon_{k,P,n}\}$ and affected by a common carrier phase error due to the frequency offset Δf. $\mathbf{N}_{k,n}$ is the additive noise plus interference matrix. $\mathbf{D}_{k,n} = [D_{k,1,n}, ..., D_{k,P,n}]$ is the time response matrix, where

$$\begin{aligned} D_{k,p,n} &= \mathcal{F}(\tau_{p,n}) \\ &= e^{-j2\pi k\frac{\lambda\tau_{p,n}}{T_{MC}}}[\rho_c(-\tau_{p,n}), \rho_c(T_c/k_s - \tau_{p,n})e^{j2\pi k\frac{\lambda}{Lk_s}} \\ &\quad , \ldots, \rho_c((Lk_s-1)T_c/k_s - \tau_{p,n})e^{j2\pi k\frac{\lambda(Lk_s-1)}{Lk_s}}]^T \end{aligned} \tag{8}$$

is the time-delay impulse response of path p sampled at T_c/k_s on the k-th subcarrier, where $\rho_c(t)$ is the correlation function of the chip pulse. The matrices $\mathbf{Z}_{k,n}$, $\mathbf{H}_{k,n}$ and $\mathbf{N}_{k,n}$ are transformed into (MLk_s)-dimensional vectors by concatenating their columns, yielding

$$\underline{Z}_{k,n} = \underline{H}_{k,n}s_{k,n} + \underline{N}_{k,n}, \tag{9}$$

where $\underline{Z}_{k,n}$, $\underline{H}_{k,n}$ and $\underline{N}_{k,n}$ denote the resulting vectors. This equation provides a new data block model for MC-CDMA systems referred to as MC-PCM. At first glance, it is similar in structure to the PCM derived for DS-CDMA in [11]. However, transition to the multi-carrier case is neither straightforward nor intuitive and requires nontrivial mathematical derivations [24]. Additionally, the CFO was not considered in the previous single-carrier model to tackle the problem of frequency synchronization. Most importantly, significant differences remain between MC-PCM and PCM. Because of the sensitivity of MC-CDMA to the CFO, we reformulated the spatial-response matrix $\mathbf{J}_{k,n}$ to include the effect of CFO. Furthermore, note that the time-response matrix $\mathbf{D}_{k,n}$, unlike its single-carrier counter-part, is carrier dependent. This makes the direct implementation of the original time-delay tracking procedure of STAR impossible for MC-CDMA systems without appropriate modifications. Based on the new MC-PCM model, we will introduce in the next section the new MC-STAR.

III. Proposed Multicarrier CDMA Spatio-Temporal Array-Receiver: MC-STAR

The block diagram of MC-STAR operations is illustrated in Fig. 3. While the proposed MC-STAR is an extension of the receiver proposed for DS-CDMA [11], it is not simply a STAR placed on each parallel subcarrier. MC-STAR implements joint space-time-frequency processing over the despread data to improve the spectrum efficiency of the MC-CDMA system. The blind channel identification and equalization as well as the acquisition and the tracking of multipaths and CFO are carried out on each subcarrier. However, their modules are interconnected to ensure proper information exchange and joint processing over carriers[6]. Mathematical details of the different procedures and their connections (shown in Fig. 3) are provided in section III-B. In the next section, we explain the concept and the advantages of the proposed receiver following the steps detailed in Table I.

A. The General Concept of MC-STAR

Starting with the original STAR, we describe the intermediate stages in our development that led to the proposed MC-STAR receiver. The core idea of the original STAR is the following (see step 0 in Table I): A main channel estimation module, referred to as decision feedback identification (DFI)

[4]Inter-symbol interference (ISI) could be eliminated by using a guard interval $T_g > \Delta\tau$, but this causes a constant capacity loss.

[5]We drop $Z_{k,l}(t)$ over the time interval $t \in [T_{MC},\ T_G)$.

[6]The complexity of MC-STAR, which is approximately the complexity of STAR multiplied by the number of subcarriers, can be assessed using the results established in [22]. The latter suggest that MC-STAR can be implemented today on a single FPGA.

TABLE I

THE GENERAL CONCEPT OF THE PROPOSED MC-STAR RECEIVER ($\mathcal{A}$, $\mathcal{S}$ AND $\mathcal{LR}$ OPERATORS STAND FOR ANALYSIS, SYNTHESIS, AND LINEAR REGRESSION, RESPECTIVELY).

Step 0: Original STAR
Analysis: $\left(\hat{\mathbf{J}}_{n+1}, (\hat{\tau}_{1,n+1}, \ldots, \hat{\tau}_{p,n+1} = \mathcal{LR}(\tilde{D}_{p,n+1}), \ldots, \hat{\tau}_{P,n+1})\right) = \mathcal{A}(\tilde{\mathbf{H}}_{n+1})$
Synthesis: $\hat{\mathbf{H}}_{n+1} = \mathcal{S}\left(\hat{\mathbf{J}}_{n+1}, \hat{\mathbf{D}}_{n+1}^T = [\ldots, \mathcal{F}(\hat{\tau}_{p,n+1}), \ldots]\right)$
Step 1: Extension to multi-carrier CDMA
Analysis: $\left(\hat{\mathbf{J}}_{k,n+1}, (\hat{\tau}_{k,1,n+1}, \ldots, \hat{\tau}_{k,p,n+1} = \mathcal{LR}(\tilde{D}^c_{k,p,n+1}), \ldots, \hat{\tau}_{k,P,n+1}\right) = \mathcal{A}(\tilde{\mathbf{H}}_{k,n+1})$
Synthesis: $\hat{\mathbf{H}}_{k,n+1} = \mathcal{S}\left(\hat{\mathbf{J}}_{k,n+1}, \hat{\mathbf{D}}_{k,n+1}^T = [\ldots, \mathcal{F}(\hat{\tau}_{k,p,n+1}), \ldots]\right)$
Step 2: Extension to joint time and frequency synchronization
Analysis: $\left(\hat{\mathbf{J}}_{k,n+1}, (\hat{\tau}_{k,1,n+1}, \ldots, \hat{\tau}_{k,p,n+1} = \mathcal{LR}(\tilde{D}^c_{k,p,n+1}), \ldots, \hat{\tau}_{k,P,n+1}), \underline{\widehat{\Delta f}_{k,n+1} = \mathcal{LR}(\hat{\mathbf{J}}_{k,n+1})}\right) = \mathcal{A}(\tilde{\mathbf{H}}_{k,n+1})$
Synthesis: $\hat{\mathbf{H}}_{k,n+1} = \mathcal{S}\left(\hat{\mathbf{J}}_{k,n+1}, \hat{\mathbf{D}}_{k,n+1}^T = [\ldots, \mathcal{F}(\hat{\tau}_{k,p,n+1}), \ldots]\right)$
$\underline{\dot{\mathbf{Z}}_{k,n+1} = e^{-j2\pi\widehat{\Delta f}_{k,n+1}(n+1)T}\mathbf{Z}_{k,n+1}}$
Step 3: Extension to multi-carrier CDMA with *frequency gain*
Analysis: $\left(\hat{\mathbf{J}}_{k,n+1}, (\hat{\tau}_{k,1,n+1}, \ldots, \hat{\tau}_{k,p,n+1} = \mathcal{LR}(\tilde{D}^c_{k,p,n+1}), \ldots, \hat{\tau}_{k,P,n+1}), \widehat{\Delta f}_{k,n+1} = \mathcal{LR}(\hat{\mathbf{J}}_{k,n+1})\right) = \mathcal{A}(\tilde{\mathbf{H}}_{k,n+1})$
Synthesis: $\hat{\mathbf{H}}_{k,n+1} = \mathcal{S}\left(\underline{\hat{\mathbf{J}}_{k,n+1} = \sum_{k-K_f}^{k+K_f} \frac{\hat{\mathbf{J}}_{k,n+1}}{2K_f+1}}, \hat{\mathbf{D}}_{k,n+1}^T = [\ldots, \mathcal{F}(\underline{\hat{\tau}_{p,n+1} = \sum_{-K}^{K} \frac{\hat{\tau}_{k,p,n+1}}{2K+1}}), \ldots]\right)$
$\dot{\mathbf{Z}}_{k,n+1} = e^{-j2\pi\widehat{\Delta f}_{n+1}(n+1)T}\mathbf{Z}_{k,n+1}$ where $\underline{\widehat{\Delta f}_{n+1} = \sum_{-K}^{K} \frac{\widehat{\Delta f}_{k,n+1}}{2K+1}}$

in [11], provides a coarse unconstrained estimate $\tilde{\mathbf{H}}_{n+1}$ of the spatio-temporal channel. In an analysis step, a space-time separation or decomposition of the channel follows by successive extraction of the multipath time-delays $\hat{\tau}_{p,n+1}$ (using simple linear regression (LR)), the temporal matrix $\hat{\mathbf{D}}_{n+1}$ and the spatial channel matrix $\hat{\mathbf{J}}_{n+1}$. In a synthesis step, a space-time reconstruction of the channel provides a more accurate constrained estimate $\hat{\mathbf{H}}_{n+1}$ by structure fitting along the nominal decomposition of the channel provided by the PCM model, $\hat{\mathbf{H}}_{n+1} = \hat{\mathbf{J}}_{n+1}\hat{\mathbf{D}}_{n+1}^T$. A final combining step exploits the constrained channel estimate $\hat{\mathbf{H}}_{n+1}$ to extract the signal component $\hat{s}_{n+1}$ using simple MRC. We exploit this basic structure to develop MC-STAR.

At step 1 of Table I, we extend original STAR to a multi-carrier system by placing STAR on each subcarrier. This extension is based on MC-PCM and it requires a modification of the time-delay tracking procedure. Indeed, we introduce an intermediate transformation of the time response to re-allow estimation of the multipath delays by simple linear regression.

Multi-carrier CDMA systems are very sensitive to the CFO. Therefore we further introduce joint time-delay and frequency synchronization (see step 2 in Table I). The effect of the CFO on the performance of the spatio-temporal array receiver was not addressed in [11]. The space/time separation of the channel, provided by MC-PCM, enables us to decouple time and carrier-frequency synchronization. The variation of multipath time-delays affects only the matrix $\mathbf{D}_{k,n}$ and the carrier-frequency offset affects only the phase of each coefficient of $\mathbf{J}_{k,n}$. We can hence estimate the CFO by linear regression (LR) of the phase variation of each coefficient of $\hat{\mathbf{J}}_{k,n}$, as depicted in the third stage of Table I. Once an estimate of the carrier frequency offset estimate $\widehat{\Delta f}$ is available by exploiting diversity in space, time and frequency, we implement carrier frequency offset recovery (CFOR) in a closed-loop structure, where we feed back the estimate of the frequency offset to the input of the receiver. The CFOR reduces the time-variations in the spatio-temporal propagation channel due to Δf to much weaker fluctuations due to the residual $\delta f = \Delta f - \widehat{\Delta f}$. It results in much weaker identification errors and enables further reduction of the carrier frequency estimation error δf. Simulation results reported in section V-B will later show the high stability and accuracy of the joint time and frequency synchronization module when tracking the paths and the CFO.

At this stage, the receiver still consists of independent modules on each subcarrier. The purpose of the last step (see step 3 in Table I) is to improve the performance of the overall receiver by interconnecting these modules and performing joint multi-carrier processing. We exploit the inter-carrier correlation, intrinsic to a multi-carrier system, as a type of *frequency gain* to improve the performance by joint multi-carrier channel identification and synchronization operations. Indeed, in the context of a multi-carrier system, the adjacent subcarriers are exposed to correlated fading, especially if the delay spread of the channel is relatively low, resulting in relatively large coherence bandwidth. Hence, averaging the adjacent subcarrier channel parameters should improve the BER performance when transmitting over such low-dispersive fading channels. Along this perspective, the parameters common to all subcarriers can be estimated more accurately by averaging their estimates over all subcarriers. These parameters

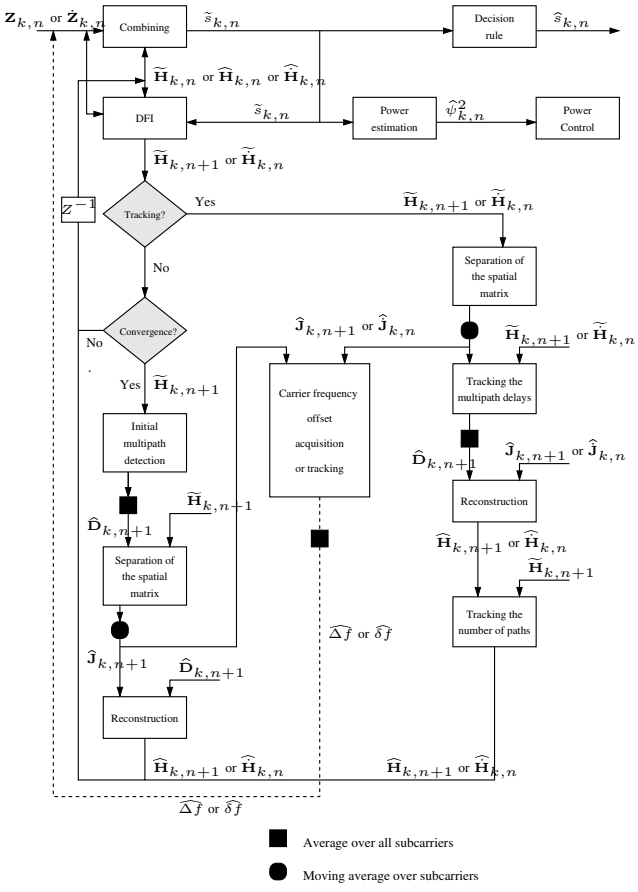

Fig. 3. Block diagram of MC-STAR.

include the number of multipaths, their corresponding time-delays and the frequency offset. Other channel parameters, such as the channel fading coefficients $\mathbf{J}_{k,n}$, are correlated but not identical over all subcarriers. Therefore, combining them may not achieve the expected performance enhancement. We thus introduce a moving average technique over subcarriers with high correlation. The fact that subcarriers are highly correlated implies similar or identical channel parameters over subcarriers. Yet, the noise is uncorrelated across subcarriers and hence the similar/common parameters can be estimated more accurately by averaging their estimates over all subcarriers, yielding the so-called *frequency gain*. The variance of the resulting estimation error is lower than the variance of the estimation error without *frequency gain*. Please bear in mind that we used the term *frequency gain* and not "frequency diversity" which relies on the fact that the fading is different over different subcarriers. Simulation results will later show that the *frequency gain* reduces the channel identification error significantly (cf. section V-C).

B. Algorithmic Implementation of MC-STAR

1) Spatio-Temporal Channel Identification and Combining: At each iteration n, we assume for each subcarrier with index k that we have an estimate $\underline{\tilde{H}}_{k,n}$ of the spatio-temporal propagation channel $\underline{H}_{k,n}$ (see Eq. (9)). From this estimate, we extract the signal component $s_{k,n}$ by spatio-temporal MRC:

$$\tilde{s}_{k,n} = \frac{\underline{\tilde{H}}_{k,n}^{H} \underline{Z}_{k,n}}{M}. \tag{10}$$

Hence, we estimate the total power received from the desired user on the k-th subcarrier for power control (PC) by $\hat{\psi}_{k,n}^2 = (1-\alpha)\hat{\psi}_{k,n-1}^2 + \alpha|\tilde{s}_{k,n}|^2$, where $\alpha \ll 1$ is a smoothing factor for power estimation. All DS-CDMA based systems (such as wideband UMTS and narrowband IS-95) require power control because it brings significant performance gains and therefore we take PC into account. Since in the case of a multi-carrier system each subcarrier is subject to different channel fading, two alternative power-control techniques can be considered. The first is per-carrier PC where we transmit more power on the subcarrier which suffers from deep fading and less power on the subcarrier which suffers from less fading. The second one is all-carrier PC where we calculate the total received power over all subcarriers and accordingly jointly decrease or increase the transmission power for all subcarriers. Simulation results not shown for lack of space confirmed that the per-carrier power control scheme performs better than the all-carrier one for both MC-DS-CDMA and MT-CDMA. Hence, in what follows, we consider only the per-carrier PC technique[7]. After power estimation, we reconstruct the differentially encoded signal estimate $\hat{s}_{k,n}$ of the signal component $s_{k,n}$ after hard decision over $\tilde{s}_{k,n}$ as:

$$\hat{s}_{k,n} = \hat{\psi}_{k,n} \arg \min_{c_m \in C_{\mathcal{M}}} \|\tilde{s}_{k,n} - c_m\|^2, \tag{11}$$

then feed it back in a decision feedback identification (DFI) scheme to update the channel estimate as follows:

$$\underline{\tilde{H}}_{k,n+1} = \underline{\tilde{H}}_{k,n} + \mu(\underline{Z}_{k,n} - \underline{\tilde{H}}_{k,n}\hat{s}_{k,n})\hat{s}_{k,n}^*, \tag{12}$$

where μ is an adaptation step-size. This DFI blind identification procedure operates as a principal eigenvector analysis technique and estimates the channel within a constellation-invariant phase ambiguity [19][8]. Since b_n is differentially encoded, this ambiguity has no consequences.

2) Time-Delay and Frequency Acquisition: In the acquisition mode, the channel identification procedure converges to a rough estimate of the spatio-temporal channel $\tilde{\mathbf{H}}_{k,n}$. From this estimate, we successively extract $\hat{\tau}_{k,p}$, $\hat{\mathbf{D}}_{k,n}$ and $\hat{\mathbf{J}}_{k,n}$ (i.e., analysis step).

Initial multipath detection: From $\tilde{\mathbf{H}}_{k,n}$, we define a localization spectrum over the possible multipath delays. Then we detect the number of multipaths $\hat{P}_k$ and estimate their time-delays $\hat{\tau}_{k,p}$ from the strongest peaks of the spectrum. We assumed earlier that the propagation time-delays are the same for all subcarriers. Therefore, we can exploit the *frequency gain* to minimize the estimation errors by averaging the localization spectra over subcarriers as follows:

$$S(lT_c) = \sum_{k=-K}^{K} S_k(lT_c)/N_c = \sum_{k=-K}^{K} \|\tilde{H}_{n,k,l}\|^2/N_c. \tag{13}$$

[7]The water filling concept could be considered, but it is beyond the scope of this paper.

[8]Note that only the DFI and the final combining step remain the same on each subcarrier (i.e., identical to original STAR [11]).

Once the number of multipath $\hat{P}$ and their time-delays $\hat{\tau}_{p,n}$ are estimated from $S(lT_c)$, we build the time-response matrix $\hat{\mathbf{D}}^T_{k,n}$ (see Eq. (8)).

Separation of the spatial response matrix $\hat{\mathbf{J}}_{k,n}$: Assuming $\tilde{\mathbf{H}}^T_{k,n} = \hat{\mathbf{H}}^T_{k,n} + \mathbf{E}_{k,n} = \hat{\mathbf{D}}_{k,n}\hat{\mathbf{J}}^T_{k,n} + \mathbf{E}_{k,n}$, where $\mathbf{E}_{k,n}$ is an estimation error matrix, we form a zero-forcing filter from $\hat{\mathbf{D}}_{k,n}$ and estimate $\tilde{\mathbf{J}}^T_{k,n} = (\hat{\mathbf{D}}^T_{k,n}\hat{\mathbf{D}}_{k,n})^{-1}\hat{\mathbf{D}}^T_{k,n}\tilde{\mathbf{H}}^T_{k,n}$. If the fading among the subcarriers is highly correlated, we can once again exploit the *frequency gain* and introduce a moving average technique over subcarriers to provide an enhanced estimate:

$$\hat{\mathbf{J}}_{k,n} = \frac{1}{2K_f+1}\sum_{k'=-K_f}^{K_f}\tilde{\mathbf{J}}_{k+k',n}, \tag{14}$$

where the averaging window span K_f determines the number of highly-correlated subcarriers to be considered in the moving average. The matrix $\hat{\mathbf{J}}_{k,n}$ is then transformed into an (MP)-dimensional vector $\underline{\hat{J}}_{k,n}$ by concatenating its columns. We represent the i-th element $\underline{\hat{J}}_{i,k,n} = \hat{r}_{i,k,n}e^{j\hat{\phi}_{i,k,n}}$ by its magnitude $\hat{r}_{i,k,n}$ and its phase $\hat{\phi}_{i,k,n}$.

Carrier frequency acquisition: We earlier assumed that the channel parameters remain unchanged over periods of, say, R symbols while a fixed phase shift (due to carrier offset) is introduced between two samples. We hence buffer the phases of each i-coefficient of $\underline{\hat{J}}_{k,n}$ over R symbols and apply a LR-based procedure to estimate Δf. For each diversity finger for $i = 1,\ldots,MP$, we form the vector $\hat{\Phi}_{i,k,nR} = [\hat{\phi}_{i,k,(n-1)R+1},\ldots,\hat{\phi}_{i,k,nR}]^T$, then estimate Δf at the symbol iteration nR as the slope of a linear regression as follows:

$$\widehat{\Delta f}_{i,k,nR} = \frac{\|R_0\|^2(R_1^T\hat{\Phi}_{i,k,nR}) - (R_1^TR_0)(R_0^T\hat{\Phi}_{i,k,nR})}{2\pi T\{\|R_0\|^2\|R_1\|^2 - (R_1^TR_0)^2\}}, \tag{15}$$

where $R_0 = [1,\ldots,1]^T$ and $R_1 = [1,\ldots,r,\ldots,R]^T$. Thus, there are MP estimates of the frequency offset for each subcarrier. We exploit space-time-frequency diversity and minimize estimation errors, by a weighted summation over these $M \times P \times N_c$ estimates:

$$\widehat{\Delta f}_{nR} = \frac{\sum_{k=-K}^{K}\sum_{i=1}^{MP}\bar{r}^2_{i,k,(n-1)R+r}\widehat{\Delta f}_{i,k,nR}}{N_c\sum_{i=1}^{MP}\bar{r}^2_{i,k,(n-1)R+r}}. \tag{16}$$

This step allows the estimation of the frequency offset while exploiting diversity over three dimensions: time, space and frequency. This idea, which was to our best knowledge first explored in the framework of this contribution [23], significantly improves the performance of MC-STAR (cf. section V-C).

3) Reconstruction of the Spatio-Temporal Channel: In the synthesis step, we reconstruct the spatio-temporal propagation matrix $\hat{\mathbf{H}}_{k,n}$ by $\hat{\mathbf{H}}_{k,n} = \hat{\mathbf{J}}_{k,n}\hat{\mathbf{D}}^T_{k,n}$. $\hat{\mathbf{H}}_{k,n}$ replaces the coarse estimate $\tilde{\mathbf{H}}_{k,n}$ and it is considered as an initial estimate for the tracking module. Once an estimate of the carrier frequency offset estimate $\widehat{\Delta f}$ is available at iteration $R+1$, we implement carrier frequency offset recovery (CFOR) in a closed-loop structure, where we feed back the estimate of the frequency offset to the input of MC-STAR:

$$\underline{\dot{Z}}_{k,n} = e^{-j2\pi\widehat{\Delta f}nT_G}\underline{Z}_{k,n} = \underline{\dot{H}}_{k,n}s_{k,n} + \underline{\dot{N}}_{k,n}, \tag{17}$$

where $\underline{\dot{H}}_{k,n}$ is the channel vector including CFOR (i.e., $\dot{\mathbf{H}}_{k,n} = \dot{\mathbf{J}}_{k,n}\mathbf{D}^T_{k,n}$) and $\underline{\dot{N}}_{k,n}$ is the interference vector within a constant phase rotation. The CFOR in Eq. (17) reduces the time-variations in $\underline{H}_{k,n}$ due to Δf to much weaker fluctuations in $\underline{\dot{H}}_{k,n}$ due to the residual $\delta f_{nR} = \Delta f_{nR} - \widehat{\Delta f}_{nR}$. Tracking of $\underline{\dot{H}}_{k,n}$ instead of $\underline{H}_{k,n}$ results in much weaker identification errors and enables further reduction of the carrier frequency estimation error δf.

4) Time-Delay and Frequency-Offset Tracking: The channel considered is time-varying. Therefore, in order to keep channel identification accurate after acquisition, we need to update the analysis/syntheis steps to the time-variations of time-delays and frequency offset. Hence, we modify the channel identification of Eq. (12) to take into account the frequency offset compensation in Eq. (17) as follows, for $n > R+1$:

$$\underline{\tilde{\dot{H}}}_{k,n+1} = \underline{\hat{\dot{H}}}_{k,n} + \mu(\underline{\dot{Z}}_{k,n} - \underline{\hat{\dot{H}}}_{k,n}\hat{s}_{k,n})\hat{s}^*_{k,n}, \tag{18}$$

where $\hat{s}_{k,n}$ is estimated by hard decision over $\tilde{s}_{k,n} = \underline{\hat{\dot{H}}}^H_{k,n}\underline{\dot{Z}}_{k,n}/M$.

The tracking module of MC-STAR repeatedly updates the number of multipaths, their time-delays and the carrier frequency offset. It allows the reconstruction of an enhanced estimate $\underline{\hat{\dot{H}}}_{k,n+1}$ from $\underline{\tilde{\dot{H}}}_{k,n+1}$ and it is implemented by the following joint time-delay and frequency tracking loop.

Tracking the number of multipaths: In order to update the identified number of multipaths, we drop or add a multipath by comparing its energy to specified thresholds [12]. For detecting a vanishing path, we only need to check if for a number of previous block iterations, the received signal power $\sum_{k=-K}^{K}\psi^2_{k,n}\epsilon^2_{k,p,n}$ continuously remains below the threshold. Note that the threshold is defined as a function of the residual noise estimate on all subcarriers. For detecting an appearing path, we check the path energy over the chip-sampled residual spectrum in [12] averaged here over all subcarriers (i.e., with *frequency gain*).

Tracking the multipath delays: We update the time response matrix $\hat{\mathbf{D}}_{k,n}$ with subspace-tracking [11]:

$$\tilde{\mathbf{D}}_{k,n+1} = \hat{\mathbf{D}}_{k,n} + \frac{\eta}{M}(\hat{\dot{\mathbf{H}}}^T_{k,n} - \hat{\mathbf{D}}_{k,n}\hat{\dot{\mathbf{J}}}^T_{k,n})\hat{\dot{\mathbf{J}}}^*_{k,n+1}, \tag{19}$$

where $\hat{\dot{\mathbf{J}}}_{k,n+1}$ is the moving average in Eq. (14) of $\tilde{\dot{\mathbf{J}}}^T_{k,n+1}$. Unlike [11], we can not implement time-delay tracking by linear regression directly over the phase of the column-wise FFT of $\tilde{\mathbf{D}}_{k,n}$ and $\widetilde{\mathbf{D}}_{k,n+1}$. Hence, we define $\tilde{\boldsymbol{\mathcal{D}}}^c_{k,n+1}$ as the column-wise FFT of $\tilde{\mathbf{D}}^c_{k,n+1}$, with p-th column $\tilde{D}^c_{k,p,n+1} = \tilde{D}_{k,p,n+1}\odot[1, e^{-j2\pi k\frac{\lambda}{Lk_s}},\ldots,e^{-j2\pi k\frac{\lambda(Lk_s-1)}{Lk_s}}]^T$, and $\hat{\boldsymbol{\mathcal{D}}}^c_{k,n}$ as the column-wise FFT of $\hat{\mathbf{D}}^c_{k,n}$, with p-th column $\hat{D}^c_{k,p,n} = \hat{D}_{k,p,n}\odot[1, e^{-j2\pi k\frac{\lambda}{Lk_s}},\ldots,e^{-j2\pi k\frac{\lambda(Lk_s-1))}{Lk_s}}]^T$, where $\odot$ denotes an element-by-element vector product. By introducing this intermediate transformation of the time responses, the p-th FFT column $\hat{\mathcal{D}}^c_{k,p,n}$ has the following nominal structure:

$$\hat{\mathcal{D}}^c_{k,p,n} \approx \left[1, e^{-j2\pi k\hat{\tau}_{k,p,n}(\frac{1}{Lk_s})},\ldots,e^{-j2\pi k\hat{\tau}_{k,p,n}(\frac{Lk_s-1}{Lk_s})}\right]^T \tag{20}$$

Hence, we can now estimate the multi-path delays $\hat{\tau}_{k,p,n+1}$ for $k = -K,\ldots,K$ and $p = 1,\ldots,\hat{P}$ by linear regressions of the phase variations between the Lk_s components of $\tilde{\mathcal{D}}^c_{k,p,n+1}$ and

$$\hat{\tau}_{k,p,n+1} = \hat{\tau}_{k,p,n} + \frac{Lk_s}{2\pi} \left\{ \frac{(Lk_s-1)\sum_{l=1}^{Lk_s}(l-1)\delta\hat{\phi}_{k,p,n,l} - \sum_{k=1}^{Lk_s}(k-1)\sum_{l=1}^{Lk_s}\delta\hat{\phi}_{k,p,n,l}}{(Lk_s-1)\sum_{l=1}^{Lk_s}(l-1)^2 - \left(\sum_{l=1}^{Lk_s}(l-1)\right)^2} \right\}. \quad (21)$$

$\hat{\mathcal{D}}^c_{k,p,n}$. If we define $\delta\hat{\phi}_{k,p,n,l} = Im\{log(\tilde{\mathcal{D}}^{c*}_{k,p,n,l}\hat{\mathcal{D}}^c_{k,p,n,l})\}$ for $l = 1, \ldots, Lk_s$, then we can estimate the multi-path delays using Eq. (21). We assumed earlier that the propagation time-delays are the same for all subcarriers. Therefore, we can once again exploit the *frequency gain* to minimize the estimation errors by averaging time-delays over carriers as follows:

$$\hat{\tau}_{p,n+1} = \sum_{k=-K}^{K} \hat{\tau}_{k,p,n+1}/N_c, \quad (22)$$

and hence we rebuild the time-response matrix $\hat{\mathbf{D}}^T_{k,n+1}$ more accurately (see Eq. (8)).

Tracking the frequency offset: Similarly to frequency offset acquisition, we estimate the carrier frequency offset error $\widehat{\delta f}_{nR}$ by linear regression over successive blocks of length R by replacing $\widehat{\Delta f}_{i,k,nR}$ and $\widehat{\Delta f}_{nR}$ by $\widehat{\delta f}_{i,k,nR}$ and $\widehat{\delta f}_{nR}$ in Eqs. (15) and (16), respectively, and $\Phi_{i,k,nR}$ by $\dot{\Phi}_{i,k,nR}$ in both equations, where $\dot{\Phi}_{i,k,nR}$ is the phase of the i-th coefficient $\hat{\underline{J}}_{i,k,n} = \hat{r}_{i,k,n}e^{j\hat{\phi}_{i,k,n}}$ of the spatial-vector $\hat{\underline{J}}_{k,n}$. The latter is derived from the spatial response matrix $\dot{\mathbf{J}}_{k,n}$ of the carrier-offset-compensated channel $\dot{\mathbf{H}}_{k,n}$. Finally, we update the frequency-offset estimate in Eq. (17) as $\widehat{\Delta f}_{nR+1} = \widehat{\Delta f}_{nR} + \widehat{\delta f}_{nR}$.

IV. Performance Analysis

The purpose of this section is to translate the link-level results into system-level results (in order to compare the performance of MT-CDMA and MC-DS-CDMA). The link-level curves provide a good picture of the performance of each system. But limiting comparisons to BER performance is not sufficient because the interference variance is not equal for all configurations.

Hence, we translate analytically the link-level simulation results into system-level results in terms of total throughput (or spectrum efficiency) under the following assumptions: 1) all users are on average received with equal power; 2) all the cells have the same average load as the target cell C; 3) the out-cell to in-cell interference ratio f is set to 0.6 [15]; 4) the chip waveform is considered a band-limited square-root raised cosine. The novelty is related to the band-limited waveform assumption. For all the MT-CDMA systems found in the literature, a time-limited waveform is generally employed [2][16][17][18]. All these papers assumed that the chip waveform is time limited to $[0, T_c]$, where T_c is the chip duration and that the system occupies an infinite bandwidth so that the chip waveform experiences no distortion during transmission. A practical system, in contrast, always involves band-limitation filtering to restrict out-of-band radiation. For example, wideband CDMA (W-CDMA) employs square-root raised cosine pulse shaping with a rolloff factor of $\beta = 0.22$. Band-limitation filtering causes the chip waveforms to disperse over the time axis and overlap one another, which would violate the assumption of the above-referenced papers. Almost no paper addressed the performance analysis of an MC-CDMA system in a band-limited chip scenario. The difficulty lies in the calculation of the variance of the interference. The exception is in [27], where recently the use of several band-limited chip waveforms for MC-DS-CDMA systems (a subclass of MC-CDMA) is considered. We derive here the interference variance of MC-CDMA (including MC-DS-CDMA and MT-CDMA) with a *band-limited* square-root raised cosine. Using the variance evaluation derived for a rectangular pulse will lead to overestimated capacity especially for MT-CDMA. We use the expression of the interference variance in the frequency domain [28]. Let $G(f)$ be the Fourier transform of the raised-cosine filter:

TABLE II
Simulation parameters.

Parameter	Value	Comment
BW_{max}	5 MHz	maximum bandwidth
M	4	number of antennas
f_c	1.9 GHz	central carrier frequency
f_D	8.8 Hz	Doppler frequency (5 kmph)
Δf	200 Hz	frequency offset
f_{PC}	1600 Hz	frequency of PC updating
Δ_{PC}	± 0.25 dB	power control adjustment
PC^{max}_{min}	± 30 dB	power control range
BER_{PC}	5%	simulated PC bit error rate
$\frac{\delta\tau}{\delta t}$	0.049 ppm	time-delay drift
$\Delta\tau$	4 chips	delay spread
R	64	regression length
β	0.22	roll-off factor
L_g	0	guard interval length

$$G(f) = \begin{cases} T_c, & 0 \le |f| \le \frac{1-\beta}{2T_c} \\ \frac{T_c}{2}\left\{1 + \cos\left[\frac{\pi T_c}{\beta}\left(|f| - \frac{1-\beta}{2T_c}\right)\right]\right\}, & \frac{1-\beta}{2T_c} \le |f| \le \frac{1+\beta}{2T_c} \\ 0, & |f| > \frac{1+\beta}{2T_c} \end{cases}. \quad (23)$$

In an interference-limited system (noise is low compared to interference), the signal to interference ratio SIR at the base-station antennas (measured by simulations) is actually $SIR = \frac{L}{(C-1)(\varsigma(\beta)+\chi(\beta))+Cf(\varsigma(\beta)+\chi(\beta))}$, where $\varsigma(\beta)$ is the normalized variance of the multiple access interference on the same carrier:

$$\varsigma(\beta) = \frac{1}{T_c}\int_{-\infty}^{\infty} G^2(f)df, \quad (24)$$

and $\chi(\beta) = \max_k[\chi_k(\beta)]$ is the normalized variance of the inter-carrier interference:

$$\chi_k(\beta) = \sum_{\substack{k'=-K \\ k'\neq k}}^{K} \frac{1}{T_c}\int_{-\infty}^{\infty} G(f)G(f-(f_k - f_{k'}))df. \quad (25)$$

It is easy to obtain $\varsigma(\beta) = (1 - \frac{\beta}{4})$. To obtain $\chi_k(\beta)$, we need to derive the integral with different frequency spacings. After

TABLE III
PARAMETERS OF EACH MULTI-CARRIER SYSTEM CONFIGURATION.

Parameter	DS-CDMA	MT-CDMA				MC-DS-CDMA				Comment
λ	-	1				L				subcarrier spacing parameter
N_c	1	3	5	7	9	3	5	7	9	number of subcarriers
L	64	128	256	384	512	64	64	64	64	spreading factor
R_c in Mcps	3.840	3.840				1.4549	0.8975	0.6488	0.5081	chip rate
P	3	3				2	1	1	1	number of paths per subcarrier
$\Delta f \times T_{MC}$	0.0033	0.0067	0.0133	0.0200	0.0267	0.0088	0.0143	0.0197	0.0252	normalized frequency offset
K_f	0	1	2	3	4	0				averaging window span in number of subcarriers
R_s in kbaud	60	90	75	70	67.5	68.2	70.15	70.97	71.45	symbol rate over all subcarriers
R_b for DBPSK in kbps	60	90	75	70	67.5	68.2	70.15	70.97	71.45	peak rate for DBPSK
R_b for DQPSK in kbps	120	180	150	140	135	136.4	140.23	141.94	142.91	peak rate for DQPSK
R_b for D8PSK in kbps	180	270	225	210	202.5	204.6	210.34	212.9	214.36	peak rate for D8PSK
BW_{nor}	1	1.013				1				bandwidth normalized vs. DS-CDMA

$$\vartheta(x) = \begin{cases} 1 - \frac{\beta}{2} - \frac{x}{2L} + \frac{3\beta}{4\pi}\sin(\frac{\pi x}{\beta L}) + (\frac{\beta}{4} - \frac{x}{4L})\cos(\frac{\pi x}{\beta L}), & \text{if } 0 \le x/L \le \min(\beta, 1-\beta) \\ 1 - \frac{x}{L} & \text{if } \beta \le x/L \le 1-\beta \text{ and } \beta < 0.5 \\ \frac{3}{4} - \frac{\beta}{4} - \frac{x}{4L} + \frac{3\beta}{4\pi}\sin(\frac{\pi x}{\beta L}) + (\frac{\beta}{4} - \frac{x}{4L})\cos(\frac{\pi x}{\beta L}) + \frac{3\beta}{8\pi}\sin(\frac{\pi x}{\beta L} - \frac{\pi}{\beta}) - & \text{if } 1-\beta \le x/L \le \beta \text{ and } \beta > 0.5 \\ (\frac{x}{8L} - \frac{1-\beta}{8})\cos(\frac{\pi x}{\beta L} - \frac{\pi}{\beta}) & \\ \frac{3}{4} + \frac{\beta}{4} - \frac{3x}{4L} + \frac{3\beta}{8L}\sin(\frac{\pi x}{\beta L} - \frac{\pi}{\beta}) - (\frac{x}{8L} - \frac{1-\beta}{8})\cos(\frac{\pi x}{\beta L} - \frac{\pi}{\beta}) & \text{if } \max(\beta, 1-\beta) \le x/L \le 1 \\ \frac{1}{4} + \frac{\beta}{4} - \frac{x}{4L} - \frac{3\beta}{8L}\sin(\frac{\pi x}{\beta L} - \frac{\pi}{\beta}) - (\frac{1+\beta}{8} - \frac{x}{8L})\cos(\frac{\pi x}{\beta L} - \frac{\pi}{\beta}) & \text{if } 1 \le x/L \le 1+\beta \\ 0 & \text{if } 1+\beta \le x/L \end{cases} \quad (26)$$

mathematical evaluations, we obtain $\chi_k(\beta) = \sum_{\substack{k'=-K \\ k' \neq k}}^{K} \vartheta(|k - k'|\lambda)$ where $\vartheta(x)$ is defined in Eq. (26). The maximum number of users that can access the system can be hence calculated (by setting $SIR = SNR_{req}$) as $C_{max} = \lfloor \frac{\frac{L}{\zeta(\beta)+\chi(\beta)} + SNR_{req}}{(1+f)SNR_{req}} \rfloor$, where $\lfloor . \rfloor$ is the floor function and SNR_{req} is the required SNR derived from link-level simulations to meet a BER of 5%. The total throughput is hence $\mathcal{T}_{max} = C_{max} \times R_b = C_{max} \times R_s \times \log_2(\mathcal{M})$, where R_b and R_s are the bit rate and the symbol rate over all subcarriers, respectively. We also define the practical spectrum efficiency as $\mathcal{E}_{max} = \mathcal{T}_{max}/BW$.[9]

V. SIMULATION RESULTS

In order to compare the performance of MT-CDMA, MC-DS-CDMA, and DS-CDMA, the fading channel parameters, the system data rate, the bandwidth, the link-level curves and the throughput must be taken into consideration. For this reason we fixed the parameters so that all three systems have the same channel parameters and almost the same bandwidth. The simulation parameters[10] common to all multi-carrier system configurations are listed in Table II. Table III shows the parameters specific to each multi-carrier CDMA configuration. We choose as a reference the DS-CDMA ($N_c = 1$) system with spreading factor $L = 64$ and chip rate of 3.84 Mcps. We assume frequency selective fading with $P = 3$ propagation paths. One of the features of MT-CDMA is that for constant bandwidth the ratio between the spreading factor L and $2K = N_c - 1$ is constant. We hence maintain the same chip rate (3.840 Mcps) by changing the spreading factor and the number of subcarriers as shown in Fig. 2. We consider four MT-CDMA configurations. Since they use the same chip rate, there are three paths in each MT-CDMA subcarrier. For a fair comparison among different configurations of MC-DS-CDMA, the bandwidth should be the same. By reducing the chip rate, we varied the number of subcarriers while maintaining the orthogonality between them, as illustrated in Fig. 2. Due to the reduction in bandwidth, each subcarrier in MC-DS-CDMA has either two paths or one path (i.e., flat fading) for $N_c = 3$ and $N_c \geq 5$, respectively. The main performance criterion is the SNR required per carrier to meet a BER of 5% in order to achieve a QoS of 10^{-6} after channel decoding. The user's data rate is calculated by adding the data rates over all subcarriers.

A. Impact of the Guard Interval on the Link-Level Performance

To illustrate the impact of the guard interval on performance, we plot in Fig. 4 the link-level curves of MT-CDMA ($N_c = 3$) and MC-DS-CDMA ($N_c = 3$, i.e., selective-channel case, see Table III) with different guard-interval lengths $L_g = 0,\ 16,$ and 32. In addition, we increased the delay spread from 4 chips, as listed in table II, to 20 chips (i.e., about 15% and 30% of the symbol duration for MT-CDMA and MC-DS-CDMA, respectively). The results show that the length of the guard interval does not affect link-level performance. They suggest that the proposed receiver does not need a guard interval to combat ISI. Indeed, MC-STAR exploits the intrinsic channel diversity by combining and equalizing the multipath signals. In order to increase spectrum efficiency, we hence eliminate the guard interval ($L_g = 0$) for the remainder of the paper.

[9]Please bear in mind that $\mathcal{E}_{max}$ is not the spectral efficiency as defined in information theory.

[10]We select $\Delta f = 200$ Hz, the maximum error tolerated by 3G standards [25], to show that even CFO residuals below the maximum value tolerated by standards result in significant losses in performance. Yet, for both low and high CFO values, the proposed CFOR module is very accurate, rapid, and efficient in compensating performance losses. For lack of space we refer the reader to [26].

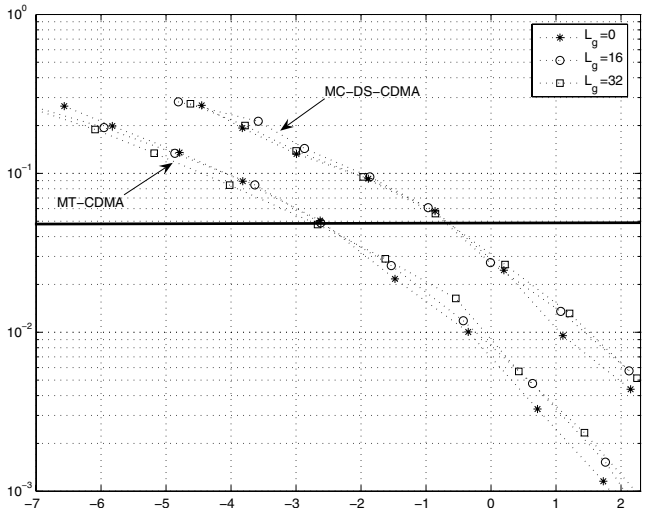

Fig. 4. BER vs. SNR in dB for MT-CDMA and MC-DS-CDMA with high delay spread ($\Delta\tau$ = 20 chips) and different guard intervals.

B. Performance Evaluation of Joint Time-Delay and Frequency-Offset Synchronization

We consider DBPSK MT-CDMA and MC-DS-CDMA modulated data with three subcarriers ($N_c = 3$). The system operates at $SNR_{in} = -3$ dB after despreading. The multipath delays in T_c are initially set to (8, 10, 12) and (4, 6) for MT-CDMA and MC-DS-CDMA, respectively. The frequency offset normalized by the subcarrier separation ($\Delta f \times T_{MC}$) is set to 0.0066 and 0.0088 for MT-CDMA and MC-DS-CDMA, respectively (i.e., $\Delta f = 200$ Hz). The performance of the joint time-delay and frequency-offset synchronization is plotted in Fig. 5. Fig. 5-a illustrates the time-delay tracking performance. It clearly shows the stability and the accuracy achieved during the tracking of the equal-power paths within a standard deviation error of 0.13 ns. In Fig. 5-b we illustrate acquisition and tracking of the frequency offset. The solid line indicates the exact value of the frequency offset. The semi-dashed curve shows that the estimated frequency offset converges relatively fast, after about 256 symbols, to the desired value within a standard deviation error of 6.5×10^{-4} (i.e., about 20 Hz). Please note that MC-STAR performs CFO acquisition and tracking for both fixed and variable CFO (see section III-B). Indeed, the fact that CFO is fixed in Fig. 5-b is not exploited by the algorithm. Actually, we selected a fixed CFO there only to focus on the acquisition and the steady-state mis-adjustment of the new joint time frequency synchronisation module. The impact of a time-varying CFO on performance is illustrated in Fig. 6. As one example, we implemented a time-varying model for both MT-CDMA and MC-DS-CDMA. Therefore, we update the frequency offset by adding RV which is a random variable uniformly distributed over $[\frac{-\Delta f}{5}, \frac{\Delta f}{5}]$. For both fixed and variable CFO values, the proposed MC-STAR is very accurate and rapid.

To illustrate the impact of speed on the performance of MC-STAR, we illustrate in Fig. 7 the acquisition and tracking of the frequency offset with high Doppler (V=100 Kmph). Note that the estimation error increases with the mobile speed. It is about 40 Hz for V=100 Kmph. The estimation error of the multipath delays remains almost the same in the presence of low or high Doppler.

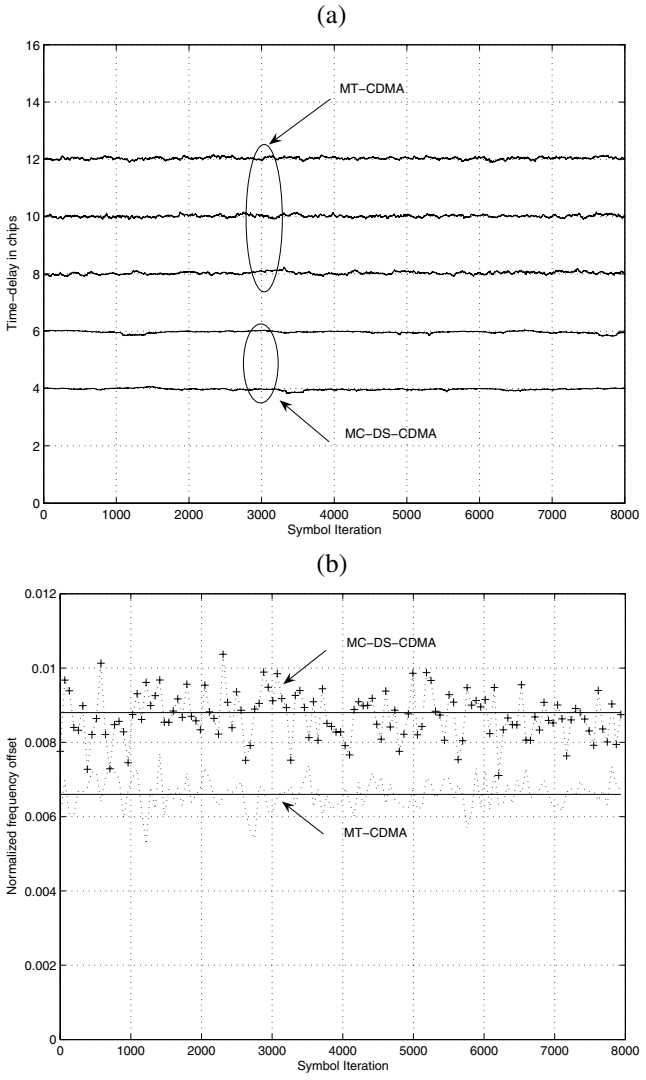

Fig. 5. Acquisition and tracking of (a): time-delays and (b): carrier frequency offset.

Concerning the convergence of DFI, Eq. (12) remains the same on each subcarrier k (identical to the single-carrier case). Therefore, the conditions of convergence, speed of convergence, and stability are identical to those of a single-carrier system [19].

C. Impact of Frequency Gain on Channel Identification Error

To evaluate the impact of the *frequency gain* on the channel identification error, we consider DBPSK MT-CDMA modulated data with five subcarriers ($N_c = 5$)[11]. In Fig. 8, we plot the average over time and over subcarriers of the channel identification error of MC-STAR with joint multi-carrier channel identification and synchronization (i.e., with *frequency gain*) for MT-CDMA ($N_c = 5$). We also plot the average identification error that would result from hypothetical application of N_c independent single-carrier STAR receivers

[11]Because of the high correlation between subcarriers, MT-CDMA benefits more from the frequency gain.

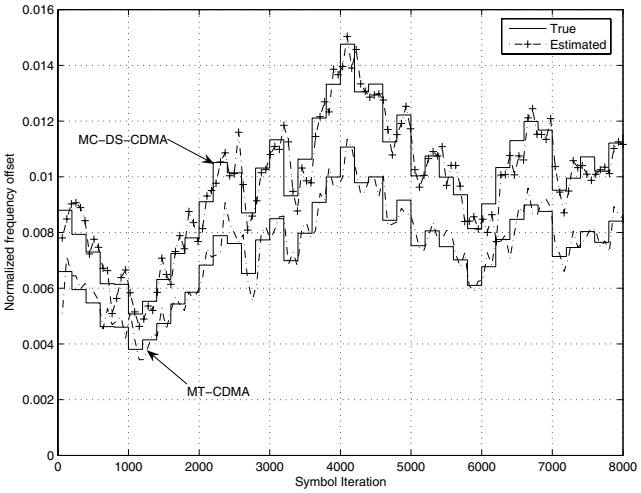

Fig. 6. Acquisition and tracking of time-varying carrier frequency offset for MT-CDMA and MC-DS-CDMA.

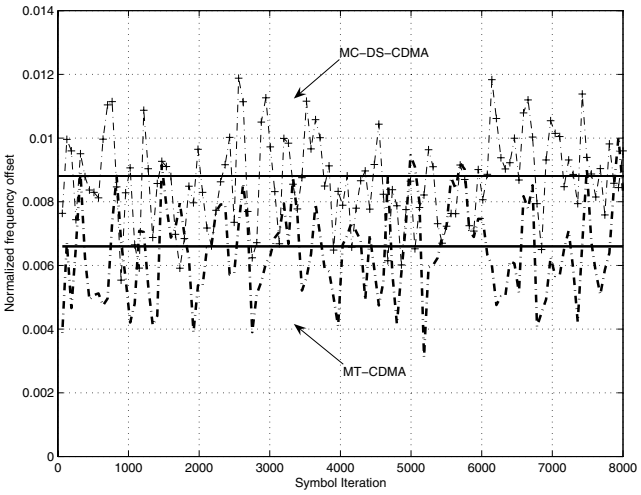

Fig. 7. Acquisition and tracking of the carrier frequency offset for MT-CDMA and MC-DS-CDMA with high Doppler (V=100 Kmph).

to the subcarriers without joint multi-carrier processing or feedback (i.e., no *frequency gain*). We compute the channel identification error by means of a scalar product, i.e., $\min \|1 \pm \underline{H}_{k,n}^{H} \widehat{\underline{H}}_{k,n}/M\|^2$. Then, we evaluate the average channel identification error by averaging over carriers and time. Simulation results show that averaging the parameters common to all subcarriers and combining the channel parameters with high correlation significantly reduce the channel identification error. The improvement in channel identification is as high as 8.5 dB for an operating SNR level of -2.9 dB (see Table IV).

D. MT-CDMA, MC-DS-CDMA, and DS-CDMA Performance Comparison

This section is dedicated to the performance comparison of MC-STAR over the DS-CDMA, MT-CDMA and MC-DS-CDMA air interfaces with DBPSK, DQPSK and D8PSK modulations. In Table IV, we provide the required SNR and the total throughput of DBPSK, DQPSK and D8PSK modulated data for DS-CDMA, MT-CDMA, and MC-DS-CDMA. First, we derive the required SNR from link-level simulations. Then,

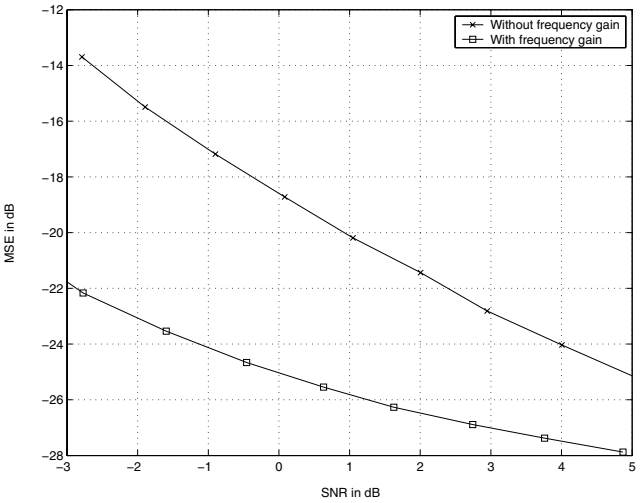

Fig. 8. Channel identification MSE in dB of MC-STAR vs. SNR in dB for MT-CDMA with and without *frequency gain*.

we translate the link-level results into system-level results using the analytical procedure in section IV. Table IV shows that for DBPSK and DQPSK modulations, when N_c is low, we can improve the system performance by increasing the number of subcarriers. But a gain saturation is encountered as the number of subcarriers increases. Indeed, with more subcarriers the inter-carrier interference becomes dominant and degrades the overall performance of the receiver, and the use of fewer subcarriers reduces the *frequency gain* and increases the channel identification error. We can conclude that for each MC-STAR configuration there exists an optimum value of N_c which results in maximum throughput. Rapid link-level deterioration is seen with D8PSK, but the deterioration is less dramatic for DS-CDMA and MC-DS-CDMA than for MT-CDMA. Indeed, higher-order modulation is more sensitive to the residual frequency offsets after recovery. In a multi-carrier environment the residual-frequency offsets for each subcarrier accumulate in the reconstructed data before detection. This process destroys the orthogonality of subcarriers and makes accurate symbol detection difficult to achieve for high-order modulations, especially when the number of subcarriers is large[12]. Single-carrier DS-CDMA, not affected by this phenomenon, has the best performance for D8PSK modulation. This degradation is smaller for MC-DS-CDMA than for MT-CDMA because the subcarrier spacing is higher. We also observe that MT-CDMA outperforms MC-DS-CDMA with DBPSK and DQPSK modulations when the number of subcarriers is low. Indeed, the BER improvement due to using longer spreading sequences and exploiting the inter-carrier correlation or *frequency gain* is higher than the degradation caused by the inter-carrier interference. Moreover, due to the reduced subcarrier bandwidth, MC-DS-CDMA has less multipath diversity, while MT-CDMA is better able to exploit path diversity and achieves better performance. The current trend is to design radio air-interfaces with flat fading subcarriers. In contrast, with MC-STAR we show that the

[12]In an ongoing study, we are investigating the incorporation of inter-carrier-interference suppression to allow a more efficient MC-STAR implementation with high-order modulations.

TABLE IV

REQUIRED SNR, CAPACITY, MAXIMUM THROUGHPUT, AND SPECTRUM EFFICIENCY OF DS-CDMA, MT-CDMA, AND MC-DS-CDMA WITH JOINT TIME AND FREQUENCY SYNCHRONIZATION FOR DBPSK, DQPSK, AND D8PSK (BEST PERFORMANCE VALUES FOR EACH MODULATION ARE IN BOLD).

MC-STAR configuration	DS-CDMA	MT-CDMA				MC-DS-CDMA			
N_c	1	3	5	7	9	3	5	7	9
Modulation	DBPSK								
SNR_{req} in dB	-1.85	-2.4	**-2.85**	-2.4	-1.65	-0.85	-1	-0.92	-0.55
C_{max}	61	49	**65**	63	55	46	48	47	43
$\mathcal{T}_{max}$ in kbps	3660	4410	**4875**	4410	3712.5	3137.1	3365.5	3335.6	3.0725
$\mathcal{E}_{max}$ in bps/Hz	0.78	0.94	**1.04**	0.94	0.79	0.67	0.72	0.71	0.66
Modulation	DQPSK								
SNR_{req} in dB	1.35	0.73	**0.5**	1.48	3.4	2.2	2.1	2.6	2.8
C_{max}	29	24	**30**	26	17	23	24	21	20
$\mathcal{T}_{max}$ in kbps	3840	4320	**4500**	3640	2295	3137.1	3365.5	2980.7	2858.1
$\mathcal{E}_{max}$ in bps/Hz	0.74	0.92	**0.96**	0.77	0.49	0.67	0.72	0.64	0.61
Modulation	D8PSK								
SNR_{req} in dB	**5.3**	6.35	7	9.5	12.8	6.82	6.8	7.2	7.6
C_{max}	**12**	7	7	4	2	8	8	7	7
$\mathcal{T}_{max}$ in kbps	**2160**	1890	1575	840	405	1636.8	1682.8	1490.4	1500.5
$\mathcal{E}_{max}$ in bps/Hz	**0.46**	0.40	0.34	0.18	0.09	0.35	0.36	0.32	0.32

positive effects of multipath diversity and *frequency gain* over large strongly-overlapping subcarriers is more significant than the negative effects of multipath and multi-carrier interference. Only when the number of subcarriers is high enough that the inter-carrier interference becomes dominant especially for high-order modulations (i.e., D8PSK) and only then MC-DS-CDMA outperforms MT-CDMA because it is more robust to inter-carrier interference.

The throughput results show that D8PSK is the least spectrum-efficient (cf. footnote 9) modulation scheme for all MC-STAR configurations. In Table IV we highlight the most spectrum-efficient MC-STAR configuration for each modulation scheme. For DBPSK and DQPSK, MT-CDMA has the best link-level performance and the highest throughput. MT-CDMA with five subcarriers outperforms all other configurations for DBPSK and DQPSK. It provides a bandwidth efficiency up to 33% higher than that achievable with single-carrier CDMA over the same channel. For D8PSK modulation, single-carrier DS-CDMA has the best performance.

VI. CONCLUSIONS

In this contribution we proposed a spectrum-efficient receiver for multi-carrier systems named MC-STAR. It performs blind channel identification and equalization as well as fast and accurate joint synchronization in time and frequency using a simple linear regression approach. MC-STAR supports both the MT-CDMA and MC-DS-CDMA air interfaces. We analyzed its performance in an unknown time-varying Rayleigh channel with multipath, carrier offset and cross-correlation between subcarrier channels. Simulations results confirm that for each MC-STAR configuration and propagation environment there exists an optimum number of subcarriers which results in maximum throughput. A higher number of subcarriers increases the inter-carrier interference, while a lower number of subcarriers reduces the *frequency gain* and increases the channel identification error. The simulations also confirm the advantages of MT-CDMA in increasing throughput and bandwidth efficiency. With four receiving antennas and five MT-CDMA subcarriers in 5 MHz bandwidth, MC-STAR provides about 1 bps/Hz at low mobility for DBPSK. This bandwidth efficiency is 33% higher than that achievable with single-carrier CDMA for DBPSK.

REFERENCES

[1] S. Hata and R. Prasad, "Overview of multicarrier CDMA," *IEEE Commun. Mag.*, vol. 35, no. 12, pp. 126-133, Dec. 1997.

[2] Y. Lie-Liang and L. Hanzo, "Performance of generalized multicarrier DS-CDMA over Nakagami-m fading channels," *IEEE Trans. Commun.*, vol. 50, no. 6, pp. 956-966, June 2002.

[3] H. Steendam and M. Moeneclaey, "The effect of carrier frequency offsets on downlink and uplink MC-DS-CDMA," *IEEE J. Sel. Areas Commun.*, vol. 19, no. 12, pp. 2528-2536, Dec. 2001.

[4] Y. Li and X. Gui, "Effect of timing and frequency offset errors on the performance of MC-CDMA systems over correlated fading channels," *IEEE International Symposium on Consumer Electronics*, paper no. ISCE03046, Dec. 2003.

[5] W. Nabhane and H. V. Poor, "Blind joint equalization and multiuser detection in dispersive MC-CDMA/MC-DS-CDMA/MT-CDMA channels," in *Proc. MILCOM 2002*, vol. 2, pp. 814-819.

[6] Q. Tian and K. Ben Letaief, "ML estimation and correction of frequency offset for MC-CDMA systems over fading channels," in *Proc. IEEE VTC 2001 Spring*, vol. 1, pp. 571-575.

[7] A. Feng, Q. Yin, Z. Zhao, and H. Zhang, "Blind space-time equalization/decoding with carrier frequency synchronization in multicarrier CDMA systems," in *Proc. IEEE International Symposium on Circuits and Systems 2002*, vol. 2, pp. 500-503.

[8] A. Feng, Q. Yin, and K. Deng, "Blind channel estimation in synchronous MC-CDMA system with consideration of carrier offset compensation," in *Proc. IEEE VTC 2002 Spring*, vol. 2, pp. 660-664.

[9] J.-H. Deng and T.-S. Lee, "An iterative maximum SINR receiver for multicarrier CDMA systems over a multipath fading channel with frequency offset," *IEEE Trans. Wireless Commun.*, vol. 2, no. 3, pp. 560-569, May 2003.

[10] D. Darsena and F. Verde, "Time-frequency synchronisation algorithm for MC-CDMA systems in LMDS applications," *Electron. Lett.*, vol. 39, no. 10, pp. 806-807, May 2003.

[11] S. Affes and P. Mermelstein, "A new receiver structure for asynchronous CDMA: STAR the spatio-temporal array-receiver," *IEEE J. Sel. Areas Commun.*, vol. 16, no. 8, pp. 1411-1422, Oct. 1998.

[12] K. Cheikhrouhou, S. Affes, and P. Mermelstein, "Impact of synchronization on performance of enhanced array-receivers in wideband CDMA networks," *IEEE J. Sel. Areas Commun.*, vol. 19, no 12, pp. 2462-2476, Dec. 2001.
[13] Z. Guozhen and L. Cong,"Performance evaluation for band-limited DS-CDMA systems based on simplified improved Gaussian approximation," *IEEE Trans. Commun.*, vol. 51, no. 7, pp. 1204-1213, July 2003.
[14] H. H. Nguyen, "Effect of chip waveform shaping on the performance of multicarrier CDMA systems," *IEEE Trans. Veh. Technol.*, vol. 54, no. 3, pp. 1022-1029, May 2005.
[15] T. S. Rappaport, *Wireless Commmunications: pPrinciples & Practice*. Prentice Hall PTR, 1999.
[16] Y. Lie-Liang and L. Hanzo, "Performance of generalized multicarrier DS-CDMA using various chip waveforms," *IEEE Trans. Commun.*, vol. 51, no. 5, pp. 748-752, May 2003.
[17] L. Vandendorpe, "Multitone spread spectrum multiple access communications system in a multipath Rician fading channel," *IEEE Trans. Veh. Technol.*, vol. 44, no. 2, pp. 327-337, May 1995.
[18] Q. M. Rahman and A. B. Sesay, "Performance analysis of MT-CDMA system with diversity combining," in *Proc. IEEE MILCOM 2001*, vol. 2, pp. 1360-1364.
[19] S. Affes and P. Mermelstein, "Adaptive space-time processing for wireless CDMA," *book chapter, Adaptive Signal Processing: Application to Real-World Problems*, J. Benesty and A. H. Huang, Eds. Berlin: Springer, 2003.
[20] W. C. Jakes, *et al.*, *Microwave Mobile Communications*. New York: Wiley, 1974.
[21] B. Natarajan, C. R. Nassar, and V. Chandrasekhar, "Generation of correlated Rayleigh fading envelopes for spread spectrum applications," *IEEE Commun. Lett.*, vol. 4, no.1 , pp. 9-11, Jan. 2000.
[22] S. Jomphe, K. Cheikhrouhou, J. Belzile, S. Affes, and J-C. Thibault, "Area-efficient advanced multiuser WCDMA receiver," invited paper, *IEEE Northeast Workshop on Circuits and Systems NEWCAS'05*, pp. 296-299.
[23] B. Smida, S. Affes, J. Li, and P. Mermelstein, "Multicarrier-CDMA STAR with time and frequency synchronization," in *Proc. IEEE ICC 2005*, vol. 4, pp. 2493-2499.
[24] J. Li, *Multitone-CDMA Array Receiver for Increased Spectrum Efficiency over Broadband Channels*, MSc dissertation, INRS-EMT, Ref. 806, 2003.
[25] 3GPP TS 25.101 V5.4.0, 3rd Generation Partnership Project (3GPP), Technical Specification Group (TSG), Radio Access Network (RAN), UE Radio Transmission and Reception (FDD), Sept. 2002.
[26] B. Smida, S. Affes, and P. Mermelstein, "Joint time-delay and frequency offset synchronization for CDMA array-receivers," in *Proc. IEEE SPAWC 2003*, pp. 499-504.
[27] S. Kondo and B. Milstein, "Performance of multicarrier DS CDMA systems," *IEEE Trans. Commun.*, vol. 44, no. 2, pp. 238-246, Feb. 1996.
[28] B. Smida and S. Affes, "Performance analysis of band-limited generalized multicarrier CDMA Systems," in *Proc. IEEE VTC 2006 Fall*, pp. 1-5.

Besma Smida (S98-M06) received the Diplôme d'Ingénieur degree in telecommunications from École Supérieure des Communications de Tunis, Tunisia, in 1995 and the M. Sc. and Ph. D. degrees in telecommunications from INRS-EMT, University of Quebec, Montreal, Canada, in 1998 and 2006. From 1998 to 1999, she worked as a research assistant in the Personal Communications Group of INRS-EMT. From 1999 to 2002, she was a research engineer in the Technology Evolution and Standards group of Microcell Solutions, Montreal, surveying and studying radio-communication technology evolution. She also took part in major wireless normalization committees (3GPP, T1P1).

She is currently a Post-doctorate Fellow at the School of Engineering and Applied Sciences, Harvard University, Cambridge, USA. Her current research interests include multicarrier modulation, spread spectrum, and network-aware application.

Sofiène Affès (S'94, M95, SM04) received the Diplôme d'Ingénieur in electrical engineering in 1992, and the Ph.D. degree with honors in signal processing in 1995, both from the École Nationale Supérieure des Télécommunications (ENST), Paris, France.

He has been since with INRS-EMT, University of Quebec, Montreal, Canada, as a Research Associate from 1995 till 1997, then as an Assistant Professor till 2000. Currently he is an Associate Professor in the Wireless Communications Group. His research interests are in wireless communications, statistical signal and array processing, adaptive space-time processing and MIMO. From 1998 to 2002 he has been leading the radio-design and signal processing activities of the Bell/Nortel/NSERC Industrial Research Chair in Personal Communications at INRS-EMT, Montreal, Canada. Currently he is actively involved in a major project in wireless of PROMPT-Qubec (Partnerships for Research on Microelectronics, Photonics and Telecommunications).

Professor Affes is the co-recipient of the 2002 Prize for Research Excellence of INRS and currently holds a Canada Research Chair in High-Speed Wireless Communications. He served as a General Co-Chair of the IEEE VTC'2006-Fall conference, Montreal, Canada, and currently acts as a member of Editorial Board of the *Wiley Journal on Wireless Communications & Mobile Computing*.

Jun Li formerly majored in mathematical theory of fractal geometry, and he obtained a Ph.D. in mathematics from the University of Montreal. He got another Master degree in telecommunications from INRS-EMT, University of Quebec in 2003. He is now an associate member of the Centre de Recherches Mathématiques, University of Montreal.

Paul Mermelstein (S58-M63-SM77-F94) received the B.Eng. degree in engineering physics from McGill University, Montreal, QC, Canada, in 1959, and the S.M., E.E., and D.Sc. degrees in electrical engineering from the Massachusetts Institute of Technology, Cambridge, in 1960, 1963, and 1964, respectively. From 1964 to 1973, he was a member of the Technical Staff in the Speech and Communications Research Department of Bell Laboratories, Murray Hill, NJ. From 1973 to 1977, he was a member of the Research Staff at Haskins Laboratories, , where he was conducting research in speech analysis, perception, and recognition. From 1977 to 1994, he was with Bell Northern Research, where he held a variety of management positions leading research and development activities in speech recognition, speech coding, and personal communications. From 1994 to 2000, he was the Leader of the major program in personal and mobile communications of the Canadian Institute for Telecommunications Research. From 1994 to 2003, he held the Bell/Nortel/NSERC Industrial Research Chair in Personal Communications at INRS-EMT, University of Quebec, Montreal, where he is now Professor Emeritus.

Since 2004 Dr. Mermelstein has also served as adjunct professor of Electrical Engineering at the University of Miami, Coral Gables. FL.